X-ray and Molecular Structure of the Diastereomeric Pair [Λ-Co(en)$_3$][Δ-Co(en)(ox)$_2$]I$_2$·3H$_2$O and [Δ-Co(en)$_3$][Δ-Co(en)(ox)$_2$]I$_2$·H$_2$O and Comparisons with [Λ-Co(en)$_3$][Δ-Co(gly)(ox)$_2$]I·H$_2$O

A. Graham Lappin,* Kenneth J. Haller, Robert M. L. Warren, and Akira Tatehata

Department of Chemistry and Biochemistry, University of Notre Dame, Notre Dame, Indiana 46556

Received March 24, 1993®

The structures of the diastereomeric pair [Λ-Co(en)$_3$][Δ-Co(en)(ox)$_2$]I$_2$·3H$_2$O and [Δ-Co(en)$_3$][Δ-Co(en)(ox)$_2$]-I$_2$·H$_2$O and the salt [Λ-Co(en)$_3$][Δ-Co(gly)(ox)$_2$]I·H$_2$O have been determined by X-ray crystallography. [Λ-Co(en)$_3$][Δ-Co(en)(ox)$_2$]I$_2$·3H$_2$O crystallizes in the monoclinic space group $P2_1$ (No. 4) with $Z = 2$, $a = 11.270(1)$ Å, $b = 9.318(1)$ Å, $c = 13.070(2)$ Å, $\beta = 100.68(1)°$, and $R = 0.032$ for 6825 reflections. [Δ-Co(en)$_3$][Δ-Co(en)(ox)$_2$]I$_2$·H$_2$O crystallizes in the orthorhombic space group $P2_12_12_1$ (No. 19) with $Z = 4$, $a = 10.773(1)$ Å, $b = 12.894(1)$ Å, $c = 18.941(3)$ Å, and $R = 0.058$ for 6339 reflections. [Λ-Co(en)$_3$][Δ-Co(gly)(ox)$_2$]I·H$_2$O crystallizes in the orthorhombic space group $P2_12_12_1$ (No. 19) with $Z = 4$, $a = 10.332(1)$ Å, $b = 10.670(2)$ Å, $c = 21.488(3)$ Å, and $R = 0.039$ for 5818 reflections. Comparison of the modes of crystal packing with a description of the ion-pairing interaction obtained from solution studies provides insight into the mechanism of chiral discrimination, particularly the role of hydrogen bonding. The importance of hydrogen bonding and electrostatic attraction in determining the nature of these interactions and the mechanism of chiral discrimination is discussed.

Introduction

Over the past decade, work in this laboratory has focused on the elucidation of chiral induction in electron-transfer reactions involving metal ion complexes.[1] A number of factors such as the charge on the ions,[2] steric hindrance,[3] the reaction medium,[4,5] and hydrogen bonding[3,4,6-8] which affect this phenomenon have been investigated. In the last case, it has been shown that changes in the pattern of hydrogen bonding between reactants have a significant effect on the electron transfer process.[3,7] In particular, reactions of [Co(en)$_3$]$^{2+}$ with oxidants such as [Co(gly)(ox)$_2$]$^{2-}$ that have an unhindered pseudo-C_3 carboxylate face available for hydrogen bonding are energetically favored when compared with oxidants such as [Co(en)(ox)$_2$]$^-$ which lack this motif (Figure 1).[7] Further, stereoselectivities in the electron transfer process are enhanced when the C_3 motif is present. Comparisons of the chiral induction in these electron transfer reactions with chiral recognition in ion pair formation between isostructural analogues which serve as a model for the electron transfer precursor complex are also revealing. While chiral induction and chiral recognition have the same sense when the C_3 motif is present, they have the opposite sense when it is absent.

The role of hydrogen bonding interactions in chiral discrimination between complex ions has proved difficult to decipher. Extensive studies of ion pairing by conductivity and chromatographic methods have been undertaken.[9,10] However, structural information on such interactions, essential to any detailed understanding of chiral induction, is not extensive. Reports are confined to the determination of a small number of ion pair structures in solution by NMR[7,11] and to a limited number of X-ray stuctures of salts containing complex cations and complex anions.[12-17]

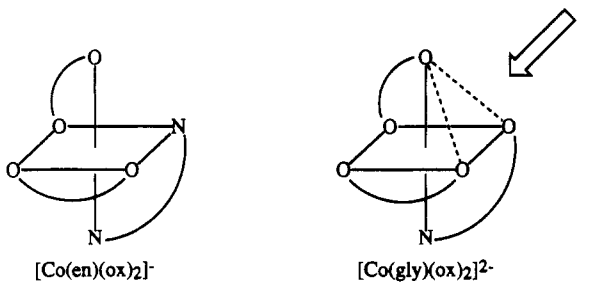

Figure 1. [Co(en)(ox)$_2$]$^-$ and [Co(gly)(ox)$_2$]$^{2-}$ showing the unhindered pseudo-C_3 carboxylate face.

This paper reports the crystal structures of a pair of diastereomers, [Λ-Co(en)$_3$][Δ-Co(en)(ox)$_2$]I$_2$·3H$_2$O and [Δ-Co(en)$_3$]-[Δ-Co(en)(ox)$_2$]I$_2$·H$_2$O, lacking the C_3 motif, and for comparison the structure of [Λ-Co(en)$_3$][Δ-Co(gly)(ox)$_2$]I·H$_2$O, where the C_3 motif is present and the charge product has been increased. It was hoped that from the examination of the solid-state structures of diastereomeric salts, some information on the mechanism of chiral discrimination between these complexes might be forthcoming. Any conclusions concerning interactions in solution derived from solid state structures must be drawn with considerable caution since the forces involved in crystal packing are complex. In the case of the interaction of [Co(en)$_3$]$^{3+}$ with [Co(en)(ox)$_2$]$^-$, the preferred interaction in solution is thought to involve the ΔΔ pair[10] while, with [Co(gly)(ox)$_2$]$^{2-}$, the ΔΛ pair is preferred.[10,18,19]

* Abstract published in *Advance ACS Abstracts*, September 15, 1993.

(1) Lappin, A. G.; Marusak, R. A. *Coord. Chem. Rev.* **1991**, *109*, 125–180.
(2) Warren, R. M. L.; Lappin, A. G.; Tatehata, A. *Inorg. Chem.* **1992**, *31*, 1566–1574.
(3) Osvath, P.; Lappin, A. G. *Inorg. Chem.* **1987**, *26*, 195–202.
(4) Geselowitz, D. A.; Hammershøi, A.; Taube, H. *Inorg. Chem.* **1987**, *26*, 1842–1845.
(5) Tatehata, A.; Oota, H.; Fukagawa, T.; Warren, R. M. L.; Lappin, A. G. *Inorg. Chem.* **1993**, *32*, 2433–2436.
(6) Tatehata, A.; Mitani, T. *Chem. Lett.* **1989**, 1167–1170.
(7) Warren, R. M. L.; Tatehata, A.; Lappin, A. G. *Inorg. Chem.* **1993**, *32*, 1191–1196.
(8) Marusak, R. A.; Osvath, P.; Kemper, M.; Lappin, A. G. *Inorg. Chem.* **1989**, *28*, 1542–1548.
(9) Tatehata, A.; Asaba, Y. *Bull Chem. Soc. Jpn.* **1988**, *61*, 3145–3151.
(10) Miyoshi, K.; Sakamoto, Y.; Ohguni, A.; Yoneda, H. *Bull Chem. Soc. Jpn.* **1985**, *58*, 2239–2246.
(11) Marusak, R. A.; Lappin, A. G. *J. Phys. Chem.* **1989**, *93*, 6856–6859.
(12) Butler, K. R.; Snow, M. R. *J. Chem. Soc. A* **1971**, 565–569.
(13) Butler, K. R.; Snow, M. R. *J. Chem. Soc., Dalton Trans.* **1976**, 251–258.
(14) Kuroda, R. *Inorg. Chem.* **1991**, *30*, 4954–4959.
(15) Lethbridge, J. W.; Dent Glasser, L. S.; Taylor, H. F. W. *J. Chem. Soc. A* **1970**, 1862–1866.
(16) Matsumoto, K.; Kuroya, H. *Bull. Chem. Soc. Jpn.* **1972**, *45*, 1755–1759.
(17) Yasui, T.; Okamoto, K.; Hidaka, J.; Ama, T.; Kawaguchi, H. *Bull. Chem. Soc. Jpn.* **1987**, *60*, 2573–2580.
(18) Tatehata, A.; Iiyoshi, M.; Kotsuji, K. *J. Am. Chem. Soc.* **1981**, *103*, 7391–7392.

0020-1669/93/1332-4498$04.00/0

Table I. Crystal Data and Intensity Data Collection Parameters

	$[\Lambda\text{-Co(en)}_3][\Delta\text{-Co(en)(ox)}_2]I_2\cdot 3H_2O$	$[\Delta\text{-Co(en)}_3][\Delta\text{-Co(en)(ox)}_2]I_2\cdot H_2O$	$[\Lambda\text{-Co(en)}_3][\Delta\text{-Co(gly)(ox)}_2]I\cdot H_2O$
empirical formula	$C_{12}H_{38}N_8O_{11}Co_2I_2$	$C_{12}H_{34}N_8O_9Co_2I_2$	$C_{12}H_{30}N_7O_{11}Co_2I$
fw	842.16	806.13	693.18
cryst dimens, mm	0.30 × 0.35 × 0.43	0.27 × 0.30 × 0.54	0.10 × 0.33 × 0.45
color	ruby red	burgundy red	violet
space group	$P2_1$ (No. 4)	$P2_12_12_1$ (No. 19)	$P2_12_12_1$ (No. 19)
a, Å	11.270(1)	10.773(1)	10.332(1)
b, Å	9.318(1)	12.894(1)	10.670(2)
c, Å	13.070(2)	18.941(3)	21.488(3)
β, deg	100.68(1)		
V, Å^3	1348.7(8)	2631.0(9)	2368.7(8)
Z	2	4	4
d_{calcd}, g cm^{-3}	2.07	2.04	1.94
μ(Mo Kα), cm^{-1}	35.54	36.48	27.51
no. of unique data measd	7360	7167	6463
no. of unique obsd data	6825	6339	5818
data/variable ratio	21.8	21.3	19.5
R_1	0.032	0.058	0.039
R_2	0.039	0.080	0.047
EOF	1.64	2.58	1.76

Although the ΔΛ pair is less soluble for both anions, $[Co(en)_3]^{3+}$ is an ineffective resolving agent for selective crystallization, and the salts have been prepared from optically pure starting materials.

Experimental Details

$[\Lambda\text{-}(+)_{589}\text{-Co(en)}_3]I_3\cdot H_2O$ (ϵ_{467} = 88 M^{-1} cm^{-1}, $\Delta\epsilon_{485}$ = +1.90 M^{-1} cm^{-1})[3] and $[\Delta\text{-}(-)_{589}\text{-Co(en)}_3]I_3\cdot H_2O$ were prepared as previously described.[20] $Na[Co(en)(ox)_2]\cdot H_2O$ was prepared by the method of Dwyer[21] and resolved to give $Na[\Delta\text{-}(+)_{546}\text{-Co(en)(ox)}_2]\cdot 3.5H_2O$ (ϵ_{541} = 109 M^{-1} cm^{-1}, $\Delta\epsilon_{581}$ = −2.53 M^{-1} cm^{-1})[22] with use of $[(+)_{546}\text{-Co(en)}_2(NO_2)_2]$-Br.[23] $Ba[Co(gly)(ox)_2]\cdot 0.5H_2O$[24] was converted to $Na_2[Co(gly)(ox)_2]\cdot 1.5H_2O$ with Na_2SO_4. $Ba[\Delta\text{-}(+)_{546}\text{-Co(gly)(ox)}_2]\cdot 2.5H_2O$ was prepared[24] using optically active $[(+)_{546}\text{-Co(en)}_2(ox)]I$ and converted to the more soluble $Na_2[\Delta\text{-}(+)_{546}\text{-Co(gly)(ox)}_2]\cdot H_2O$ (ϵ_{565} = 138 M^{-1} cm^{-1}, $\Delta\epsilon_{581}$ = −3.08 M^{-1} cm^{-1})[24] with use of Na_2SO_4.

Red crystals of $[\Lambda\text{-}(+)_{589}\text{-Co(en)}_3][\Delta\text{-}(+)_{546}\text{-Co(en)(ox)}_2]I_2\cdot 3H_2O$ were obtained after a solution prepared by adding 0.38 g (1 mmol) of $Na[\Delta\text{-}(+)_{546}\text{-Co(en)(ox)}_2]\cdot 3.5H_2O$ to a solution of 0.64 g (1 mmol) of $[\Lambda\text{-}(+)_{589}\text{-Co(en)}_3]I_3\cdot H_2O$ in 15 mL of water was maintained at 4 °C for several days. Red crystals of $[\Delta\text{-}(-)_{589}\text{-Co(en)}_3][\Delta\text{-}(+)_{546}\text{-Co(en)(ox)}_2]$-$I_2\cdot H_2O$ were obtained from a solution prepared by addition of 0.076 g (0.2 mmol) of $Na[\Delta\text{-}(+)_{546}\text{-Co(en)(ox)}_2]\cdot 3.5H_2O$ to a solution of 0.128 g (0.2 mmol) of $[\Delta\text{-}(-)_{589}\text{-Co(en)}_3]I_3\cdot H_2O$ in 2.5 mL of water, after warming and allowing the solution to stand for 3 h. Fine needles of $[\Lambda\text{-}(+)_{589}\text{-Co(en)}_3][\Delta\text{-}(+)_{546}\text{-Co(gly)(ox)}_2]I\cdot H_2O$ were obtained from 0.075 g (0.2 mmol) of $Na_2[\Delta\text{-}(+)_{546}\text{-Co(gly)(ox)}_2]\cdot H_2O$ added to a solution of 0.128 g (0.2 mmol) of $[\Lambda\text{-}(+)_{589}\text{-Co(en)}_3]I_3\cdot H_2O$ in 2.5 mL of water after 3 days at 4 °C. In each case the crystals were gathered by filtration and washed with water, ethanol, and ether and their compositions were checked by absorption and CD spectroscopy prior to X-ray analysis. Examination of crystals of $[\Lambda\text{-Co(en)}_3][\Delta\text{-Co(en)(ox)}_2]$-$I_2\cdot 3H_2O$, $[\Delta\text{-Co(en)}_3][\Delta\text{-Co(en)(ox)}_2]I_2\cdot H_2O$, and $[\Lambda\text{-Co(en)}_3][\Delta\text{-Co(gly)(ox)}_2]I\cdot H_2O$ was carried out at 294 ± 1 K on an Enraf-Nonius CAD4 diffractometer equipped with a graphite crystal incident beam monochromator using Mo radiation (λ = 0.710 73 Å). A summary of the crystal data and intensity collection parameters is presented in Table I.[25] Data reduction was performed by using standard programs.[26] Lorentz, polarization, and empirical absorption corrections based on ψ curves were applied to the data. All three structures were solved by the Patterson heavy-atom method followed by a series of difference electron density Fourier maps and were refined by a full-matrix least-squares process.

For $[\Lambda\text{-Co(en)}_3][\Delta\text{-Co(en)(ox)}_2]I_2\cdot 3H_2O$, a total of 7723 reflections were collected. The intensities of four representative reflections measured every 60 min did not show any systematic variation during the time required for the data collection. Transmission coefficients from absorption corrections ranged from 0.815 to 1.000. After preliminary refinement, several partially occupied water sites were located with occupancy factors 0.65 for O1s and O3s, 0.55 for O2s, 0.35 for O4s and O6s, and 0.45 for O5s so that the sum of the factors equaled 3.0. Positions for most of the hydrogen atoms could be found in a difference electron density Fourier map calculated at this point. Final cycles of least-squares refinement assigned anisotropic displacement parameters to the non-hydrogen atoms of the cobalt complexes and the iodine atoms, but isotropic displacement parameters to the disordered waters of crystallization, and included the hydrogen atom coordinates and isotropic displacement parameters as fixed parameters. The highest peak in the final difference electron density Fourier map was 2.29 e/Å^3. The highest peak not associated with the iodine atoms was 0.76 e/Å^3. Refinement of the other enantiomorph converged with R_1 = 0.038 and R_2 = 0.047, confirming the veracity of the enantiomorph reported.

For $\Delta\text{-}[Co(en)_3]\Delta\text{-}[Co(en)(ox)_2]I_2\cdot H_2O$, a total of 12941 reflections were collected. Plots of the intensities of standard reflections measured every 60 min showed a systematic decline during data collection and a linear decay correction ranging from 1.000 to 1.046 was applied to the data. Transmission coefficients from absorption corrections ranged from 0.772 to 1.000. Final cycles of refinement assigned anisotropic displacement parameters to the non-hydrogen atoms and included the hydrogen atom coordinates and isotropic displacement parameters as fixed parameters. The highest peak in the final difference electron density Fourier map was 7.2 e/Å^3. Although this value seems high, it is less than the height of a typical carbon atom and is the result of a combination of the inadequacies in the absorption correction model and the high resolution of the structure. The highest peak not associated with the iodine atoms was 1.5 e/Å^3. Refinement of the other enantiomorph converged with R_1 = 0.062 and R_2 = 0.087, confirming the veracity of the enantiomorph reported.

For $[\Delta\text{-Co(en)}_3][\Delta\text{-Co(gly)(ox)}_2]I\cdot H_2O$, a total of 6997 reflections were collected. The intensities of standard reflections measured every 60 min showed a small systematic decline, and a linear decay correction ranging from 1.000 to 1.048 was applied. Transmission coefficients from absorption corrections ranged from 0.769 to 1.000. The model for the final cycles of refinement assigned anisotropic displacement parameters to all non-hydrogen atoms and included the hydrogen atom coordinates and isotropic displacement parameters as fixed parameters. The highest peak in the final difference electron density Fourier map was 3.48 e/Å^3.

(19) Tatehata, A.; Fujita, M.; Ando, K.; Asaba, Y. *J. Chem. Soc., Dalton Trans.* **1987**, 1977–1982.
(20) Broomhead, J. A.; Dwyer, F. P.; Hogarth, J. W.; Sievers, R. E. *Inorg. Synth.* **1960**, *6*, 183–188.
(21) Dwyer, F. P.; Reid, I. K.; Garvan, F. L. *J. Am. Chem. Soc.* **1961**, *83*, 1285–1287.
(22) Douglas, B. E.; Haines, R. A.; Brushmiller, J. G. *Inorg. Chem.* **1963**, *2*, 1194–1198.
(23) Worrell, J. H. *Inorg. Synth.* **1972**, *13*, 195–202.
(24) Yamasaki, K.; Hidaka, J.; Shimura Y. *Bull. Chem. Soc. Jpn.* **1969**, *42*, 119–126.
(25) Data were collected by the θ-2θ scan technique to a maximum 2θ value of 58.7°. Data with $F_o > 3\sigma(F_o)$ were considered observed. Hydrogen atoms were included in the final refinement cycles as idealized contributions with d(C–H) = 0.98 Å, d(N–H) = 0.87 Å, and B(H) = 1.1B(attached atom). All calculations were performed on a VAXstation 3200 using the SDP/VAX program system.
(26) Frenz, B. A. The Enraf-Nonius CAD4 SDP—A Real-Time System for Concurrent X-ray Data Collection and Crystal Structure Determination. In *Computing in Crystallography;* Schenk, H., Olthof-Hazelkamp, R., van Konigsveld, H., Bassi, G. C., Eds.; Delft University Press: Delft, Holland, 1978, pp 64–71.

The highest peak not associated with the iodine atoms was 0.71 e/Å^3. Refinement of the other enantiomorph converged with $R_1 = 0.048$ and $R_2 = 0.059$, confirming the veracity of the enantiomorph reported.

On an interpretive note, the definition of what constitutes hydrogen bonding is broad.[27] Inferences based on the positions of the heavy atoms have proved extremely useful in many studies.[28,29] Hydrogen bonds of the type O···H–O have been found to occur with an O–O distance over the range 2.4–3.2 Å, while those of the type O···H–N have been found to occur with an O–N distance over the range 2.5–3.4 Å. In this study, which focuses on the role of hydrogen bonding, the lists of possible hydrogen bonds contain no examples where the heavy atoms are greater than 3.22 Å apart. A second criterion for the presence of a hydrogen bond concerns the length of the O···H hydrogen bond itself. This is difficult to define by X-ray crystallography. The sum of the van der Waals radii of oxygen and hydrogen is about 2.7 Å,[30] and where O···H distances significantly shorter than this are observed, hydrogen bonding may be unambiguously invoked. All quoted possible hydrogen bonds have O···H distances at least 0.1 Å less than the van der Waals contact distance. These criteria are designed to be as inclusive as possible, it should therefore be emphasized that parameters close to the upper limits indicate an extremely weak interaction.

Results

Fractional crystallographic coordinates and isotropic atomic displacement parameters for the three salts are collected in Tables II–IV. The X-ray structures of all three salts contain $[Co(en)_3]^{3+}$ cations which have bond lengths and angles within normal limits.[31-39] In two cases the absolute configuration is $\Lambda(\delta\delta\delta)$ and in the other $\Delta(\lambda\lambda\lambda)$ so that all three complexes have the lel_3 conformation of the five-membered chelate rings. The complex anions also have bond lengths and angles within normal limits. The oxalate rings in all three structures are close to planarity. For the $[Co(en)(ox)_2]^-$ anions, the Co–O bonds trans to the nitrogen donors of the 1,2-diaminoethane rings average 0.024 Å longer than those trans to oxalate, a feature noted in a previous structure of this complex.[17] In $[\Lambda\text{-}Co(en)_3][\Delta\text{-}Co(en)(ox)_2]\text{-}I_2\cdot 3H_2O$, the absolute configuration of the anion is $\Delta(\lambda)$ with a lel conformation for the five-membered 1,2-diaminoethane ring while, for $[\Delta\text{-}Co(en)_3][\Delta\text{-}Co(en)(ox)_2]I_2\cdot H_2O$, the absolute configuration is $\Delta(\delta)$ with an ob conformation. The difference in the conformation of the 1,2-diaminoethane ring may be due to the presence of a hydrogen bonding interaction in the latter structure. The glycinate ring in $[\Lambda\text{-}Co(en)_3][\Delta\text{-}Co(gly)(ox)_2]I\cdot H_2O$ is best described as having an envelope conformation with C7 out of the plane of the other atoms.

A packing diagram for $[\Lambda\text{-}Co(en)_3][\Delta\text{-}Co(en)(ox)_2]I_2\cdot 3H_2O$ is shown in Figure 2. The $[Co(en)_3]^{3+}$ ions lie with their C_3 axes close to the crystallographic *b* axis and separated by I2. The $[Co(en)(ox)_2]^-$ ions have a similar arrangement with their C_2 axes close to the crystallographic *a* axis, and separated by I1. The hydrogen-bonding network extends in two-dimensional sheets along the b and c axes of the crystal. These sheets stack on top of each other along the *a* axis of the crystal, and there is no hydrogen bonding between the sheets, even through solvent molecules. Four different cation–anion hydrogen bonding interactions are observed. At the shortest Co–Co distances of 6.13 and 6.15 Å, weak hydrogen bonding occurs through one metal-bound and one terminal oxygen atom of oxalate with two of the three available protons on one of the C_3 faces of a $[Co(en)_3]^{3+}$ ion (Figure 3a). At longer Co–Co distances of 7.53 and 7.55 Å, the terminal oxygen atoms of oxalate interact with the two available protons along one of the three C_2 axes of a $[Co(en)_3]^{3+}$ ion (Figure 3b). These hydrogen bonding interactions are stronger than those for the shorter Co–Co distances. No hydrogen bonding is observed between $[Co(en)(ox)_2]^-$ complex ions. The iodide ion I1 is located along the C_2 axis of $[Co(en)_3]^{3+}$ which is not involved in hydrogen bonding and also along a pseudo-C_2 axis of $[Co(en)(ox)_2]^-$. I2 is located along the C_2 axis of $[Co(en)(ox)_2]^-$. A list of possible hydrogen-bonding interactions in $[\Lambda\text{-}Co(en)_3]\text{-}[\Delta\text{-}Co(en)(ox)_2]I_2\cdot 3H_2O$ is given in Table V.

A packing diagram for $[\Delta\text{-}Co(en)_3][\Delta\text{-}Co(en)(ox)_2]I_2\cdot H_2O$ is shown in Figure 4. The C_2 axis of $[Co(en)(ox)_2]^-$ is aligned close to the crystallographic *a* axis, along which the complex anions form a stack. A network of hydrogen bonds extends throughout the crystal in three dimensions, encompassing both complex ions. The shortest Co–Co distances occur along the C_2 axes of the

Table II. Fractional Monoclinic Coordinates and Isotropic Atomic Displacement Parameters for the Non-Hydrogen Atoms of $[\Lambda\text{-}Co(en)_3][\Delta\text{-}Co(en)(ox)_2]I_2\cdot 3H_2O$[a]

atom	*x*	*y*	*z*	B_{iso}, Å^2
Co1	0.51087(3)	0.500	0.75419(3)	1.794(6)
N1	0.6449(3)	0.3851(3)	0.7221(2)	2.49(5)
C1	0.7616(3)	0.4311(5)	0.7854(3)	3.65(9)
C2	0.7559(4)	0.5915(6)	0.8009(3)	3.90(9)
N2	0.6370(3)	0.6263(4)	0.8277(2)	2.82(6)
N3	0.3844(3)	0.6242(4)	0.7894(2)	2.92(6)
C3	0.3773(4)	0.6023(5)	0.9002(3)	3.53(8)
C4	0.3928(4)	0.4476(5)	0.9231(3)	3.41(8)
N4	0.5035(3)	0.3966(3)	0.8838(2)	2.33(5)
N5	0.3929(3)	0.3658(3)	0.6779(2)	2.47(5)
C5	0.3891(4)	0.3844(4)	0.5651(3)	3.07(7)
C6	0.3975(4)	0.5403(4)	0.5457(3)	3.14(8)
N6	0.5001(3)	0.6011(3)	0.6208(2)	2.37(5)
Co2	0.84989(3)	0.50109(7)	0.30754(3)	2.034(6)
N7	0.9737(3)	0.6255(4)	0.2757(2)	2.86(6)
C7	1.0926(4)	0.5850(5)	0.3388(4)	3.83(9)
C8	1.0913(4)	0.4232(5)	0.3468(4)	3.93(9)
N8	0.9790(3)	0.3839(4)	0.3812(2)	2.81(6)
O1	0.7329(2)	0.3776(3)	0.3515(2)	2.63(5)
C9	0.7059(3)	0.4194(4)	0.4364(3)	2.56(7)
O2	0.8415(2)	0.6112(3)	0.4270(2)	2.44(4)
C10	0.7654(3)	0.5600(4)	0.4789(3)	2.26(6)
O3	0.6368(3)	0.3582(3)	0.4852(2)	3.87(6)
O4	0.7373(2)	0.6148(3)	0.5565(2)	3.08(5)
O5	0.7285(2)	0.6183(3)	0.2244(2)	2.46(4)
C11	0.6993(3)	0.5722(4)	0.1317(3)	2.64(7)
O6	0.8477(2)	0.3918(3)	0.1855(2)	2.86(5)
C12	0.7684(3)	0.4377(4)	0.1086(3)	2.58(7)
O7	0.6254(3)	0.6254(4)	0.0616(2)	3.83(6)
O8	0.7471(3)	0.3812(4)	0.0226(2)	3.96(7)
I1	0.92035(2)	−0.00275(4)	0.33590(2)	3.408(4)
I2	0.59052(2)	0.00405(4)	0.76244(2)	3.579(4)
O1s	0.9424(9)	0.152(1)	0.0830(8)	10.4(2)[b]
O2s	1.094(1)	0.532(2)	0.095(1)	14.2(4)[b]
O3s	0.921(1)	0.705(2)	1.058(1)	14.6(4)[b]
O4s	−0.026(2)	0.219(3)	0.981(2)	13.0(7)[b]
O5s	0.139(1)	0.422(2)	1.062(1)	11.9(5)[b]
O6s	0.060(3)	0.423(4)	0.921(3)	25(1)[b]

[a] Estimated standard deviations in the least significant digits are given in parentheses. Thermal parameters for the anisotropically refined atoms are given in the form of the isotropic equivalent displacement parameter defined as $^4/_3[a^2B_{11} + b^2B_{22} + c^2B_{33} + ab(\cos\gamma)B_{12} + ac(\cos\beta)B_{13} + bc(\cos\alpha)B_{23}]$. [b] The water solvate molecules were assigned occupancy factors of 0.65 for O1s and O3s, 0.55 for O2s, 0.35 for O4s and O6s, and 0.45 for O5s. These atoms were refined with isotropic atomic displacement parameters.

(27) Joesten, M. D. *J. Chem. Educ.* **1982,** *59,* 362–366 and references therein.
(28) Hamilton, W. C.; Ibers, J. A. *Hydrogen Bonding in Solids*; W. A. Benjamin Inc.: New York, 1968; Chapter 1.
(29) Pimentel, G. C.; McClellan, A. L. *The Hydrogen Bond,* W. H. Freeman and Co.: San Francisco, CA, 1960; Chapter 9.
(30) Bondi, A. *J. Phys. Chem.* **1964,** *68,* 441–451.
(31) Nakatsu, K.; Shiro, M.; Saito, Y.; Kuroya, H. *Bull. Chem. Soc. Jpn.* **1957,** *30,* 158–164.
(32) Nakatsu, K. *Bull. Chem. Soc. Jpn.* **1962,** *35,* 832–839.
(33) Iwata, M.; Nakatsu, K.; Saito, Y. *Acta Crystallogr.* **1969,** *B25,* 2562–2571.
(34) Witiak, D.; Clardy, J. C.; Martin, D. S. *Acta Crystallogr.* **1972,** *B28,* 2694–2699.
(35) Whuler, P. A.; Brouty, C.; Spinat, P.; Herpin, P. *Acta Crystallogr.* **1975,** *B31,* 2069–2076.
(36) Whuler, P. A.; Spinat, P.; Brouty, C. *Acta Crystallogr.* **1980,** *B36,* 1086–1091.
(37) Fuertes, A.; Miravitlles, C.; Ibanez, R.; Martinez-Tamayo, E.; Beltran-Porter, A. *Acta Crystallogr.* **1988,** *C44,* 417–421.
(38) Magill, L. S.; Korp, J. D.; Bernal, I. *Inorg. Chem.* **1981,** *20,* 1187–1192.
(39) Mizuta, T.; Tada, T.; Kushi, Y.; Yoneda, H. *Inorg. Chem.* **1988,** *27,* 3836–3841.

Table III. Fractional Orthorhombic Coordinates and Isotropic Atomic Displacement Parameters for the Non-Hydrogen Atoms of $[\Delta\text{-Co(en)}_3][\Delta\text{-Co(en)(ox)}_2]I_2\cdot H_2O$[a]

atom	x	y	z	B_{iso}, Å^2
Co1	0.54310(7)	0.13927(6)	0.12786(3)	1.75(1)
N1	0.3713(5)	0.1262(4)	0.1603(3)	2.47(9)
C1	0.3679(7)	0.1388(6)	0.2394(3)	3.0(1)
C2	0.4514(7)	0.2296(6)	0.2544(3)	3.0(1)
N2	0.5716(5)	0.2136(5)	0.2168(3)	2.71(9)
N3	0.5848(5)	0.0047(4)	0.1694(3)	2.55(9)
C3	0.7130(7)	−0.0288(6)	0.1457(4)	3.5(1)
C4	0.7908(7)	0.0668(7)	0.1446(4)	3.7(1)
N4	0.7221(5)	0.1484(4)	0.1042(3)	2.49(8)
N5	0.5018(5)	0.0730(4)	0.0375(2)	2.26(8)
C5	0.460(1)	0.1530(7)	−0.0123(4)	5.3(2)
C6	0.518(1)	0.2522(7)	0.0023(4)	4.9(2)
N6	0.5137(6)	0.2701(4)	0.0779(3)	2.8(1)
Co2	0.81464(8)	0.16535(6)	0.38594(4)	2.22(1)
O1	0.8165(5)	0.0455(4)	0.4442(2)	2.67(7)
C7	0.7328(6)	−0.0211(5)	0.4259(3)	2.7(1)
O2	0.7019(5)	0.0902(4)	0.3279(2)	2.70(8)
C8	0.6645(6)	0.0049(5)	0.3550(3)	2.44(9)
O3	0.7087(5)	−0.1003(4)	0.4576(2)	3.4(1)
O4	0.5861(5)	−0.0515(4)	0.3313(2)	3.46(9)
O5	0.6769(4)	0.2211(3)	0.4371(2)	2.63(7)
C9	0.6329(6)	0.3025(5)	0.4074(3)	2.20(9)
O6	0.8011(4)	0.2814(4)	0.3265(2)	2.85(8)
C10	0.7051(6)	0.3381(5)	0.3409(3)	2.4(1)
O7	0.5380(5)	0.3488(4)	0.4256(3)	3.20(8)
O8	0.6686(6)	0.4104(4)	0.3074(3)	3.72(9)
N7	0.9325(6)	0.2370(5)	0.4447(3)	3.1(1)
C11	1.0545(8)	0.2368(8)	0.4066(4)	4.7(2)
C12	1.0706(6)	0.1361(8)	0.3739(4)	4.2(2)
N8	0.9567(7)	0.1173(6)	0.3322(3)	3.6(1)
I1	0.90957(7)	−0.18641(8)	0.29916(3)	6.19(2)
I2	0.66720(7)	0.50440(6)	−0.01020(5)	6.56(2)
O1s	−0.2517(8)	0.3697(6)	0.1537(4)	6.2(2)

[a] Estimated standard deviations in the least significant digits are given in parentheses. Thermal parameters for the anisotropically refined atoms are given in the form of the isotropic equivalent displacement parameter defined as $^4/_3[a^2B_{11} + b^2B_{22} + c^2B_{33} + ab(\cos\gamma)B_{12} + ac(\cos\beta)B_{13} + bc(\cos\alpha)B_{23}]$.

Table IV. Fractional Orthorhombic Coordinates and Isotropic Atomic Displacement Parameters for the Non-Hydrogen Atoms of $[\Delta\text{-[Co(en)}_3][\Delta\text{-Co(gly)(ox)}_2]I_2\cdot H_2O$[a]

atom	x	y	z	B_{iso}, Å^2
Co1	0.87379(5)	0.09054(4)	0.59261(2)	1.71(1)
N1	0.9754(3)	0.0440(3)	0.6662(1)	2.24(6)
C1	0.9421(4)	−0.0857(4)	0.6853(2)	3.35(8)
C2	0.7979(4)	−0.1019(4)	0.6761(2)	3.47(9)
N2	0.7697(3)	−0.0591(3)	0.6112(2)	2.63(6)
N3	0.7547(3)	0.1978(3)	0.6407(2)	2.60(6)
C3	0.7818(4)	0.3310(4)	0.6246(2)	3.07(8)
C4	0.9246(5)	0.3451(4)	0.6234(2)	3.24(8)
N4	0.9764(3)	0.2438(3)	0.5821(2)	2.40(6)
N5	0.7746(3)	0.1229(3)	0.5174(2)	2.39(6)
C5	0.8121(4)	0.0317(4)	0.4688(2)	2.79(8)
C6	0.9563(4)	0.0189(4)	0.4722(2)	2.88(7)
N6	0.9888(3)	−0.0041(3)	0.5380(2)	2.31(6)
Co2	0.87032(5)	0.56094(5)	0.32163(2)	2.07(1)
O1	0.8411(3)	0.4239(3)	0.2674(1)	2.94(6)
C9	0.9076(4)	0.4325(4)	0.2168(2)	2.60(7)
C10	1.0041(4)	0.5406(4)	0.2169(2)	2.75(8)
O2	0.9978(3)	0.6125(3)	0.2651(1)	2.96(5)
O3	0.8972(3)	0.3649(3)	0.1718(2)	3.77(7)
O4	1.0787(4)	0.5572(4)	0.1744(2)	5.29(8)
O5	0.7482(2)	0.4982(3)	0.3808(1)	2.09(5)
C11	0.7962(3)	0.4216(4)	0.4200(2)	2.18(6)
C12	0.9447(3)	0.4027(3)	0.4129(2)	2.27(6)
O6	0.9945(2)	0.4672(3)	0.3687(1)	2.60(5)
O7	0.7369(3)	0.3666(3)	0.4607(1)	2.72(5)
O8	1.0032(3)	0.3319(3)	0.4473(1)	2.86(5)
N7	0.8945(3)	0.7099(3)	0.3701(2)	2.52(6)
C7	0.7807(5)	0.7916(4)	0.3610(2)	3.08(8)
C8	0.7205(4)	0.7621(4)	0.2989(2)	2.56(7)
O9	0.7454(3)	0.6526(3)	0.2773(1)	2.74(5)
O10	0.6511(4)	0.8373(3)	0.2722(2)	4.26(7)
I	0.05438(5)	0.16441(3)	0.96797(2)	6.03(1)
O1s	0.7076(3)	0.2275(3)	0.3243(2)	4.71(8)

[a] Estimated standard deviations in the least significant digits are given in parentheses. Thermal parameters for the anisotropically refined atoms are given in the form of the isotropic equivalent displacement parameter defined as $^4/_3[a^2B_{11} + b^2B_{22} + c^2B_{33} + ab(\cos\gamma)B_{12} + ac(\cos\beta)B_{13} + bc(\cos\alpha)B_{23}]$.

$[Co(en)_3]^{3+}$ cations closest to the *c* axis of the crystal. At Co–Co distances of 5.71 and 6.23 Å, an oxalate ligand interacts through a terminal and a metal-bound oxygen atom along one of these C_2 axes (Figure 5a). Here the two sides of a single oxalate are involved in interactions with two separate cations. In addition, a terminal oxygen of this oxalate is involved in a hydrogen-bond interaction along a C_2 axis of a third $[Co(en)_3]^{3+}$ ion, at a Co–Co distance of 7.81 Å. The other oxalate hydrogen bonds only through terminal oxygen atoms, to a C_3 face of $[Co(en)_3]^{3+}$ at a Co–Co distance of 7.23 Å (Figure 5b), and to the 1,2-diaminoethane ring on a second complex anion. One of the iodide ions, I2, lies close to N6 on this face of the complex. The other C_3 face of $[Co(en)_3]^{3+}$ is hydrogen-bonded to the water of crystallization, which interacts with two of the three available protons. Both iodine atoms lie close to the van der Waals touching distance from the oxygen atom of the water molecule, and these three species together occupy a large cavity in the complex anion–cation network. I1 lies close to N8 of $[Co(en)(ox)_2]^-$. Complex anions, $[Co(en)(ox)_2]^-$, are strongly hydrogen-bonded to each other at a Co–Co distance of 7.24 Å, linking two *a*-axis stacks. A list of possible hydrogen-bonding interactions in $[\Delta\text{-Co(en)}_3]$-$[\Delta\text{-Co(en)(ox)}_2]I_2\cdot H_2O$ is given in Table VI.

A packing diagram for $[\Lambda\text{-Co(en)}_3][\Delta\text{-[Co(gly)(ox)}_2]I\cdot H_2O$ is shown in Figure 6. There are alternating stacks of complex anions and cations aligned with the crystallographic *b* axis. The iodide ions are closely associated with the cation stack. A hydrogen bonding network pervades the entire crystal. The C_3 axes of the $[Co(en)_3]^{3+}$ cations lie close to the a axis of the crystal, and it is in this direction that the closest cation–anion interactions are observed. At Co–Co distances of 5.69 and 5.75 Å, an oxalate

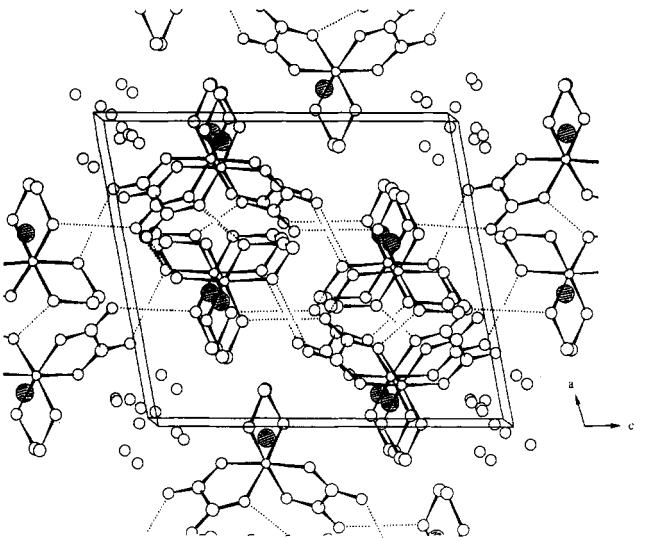

Figure 2. Packing diagram for $[\Lambda\text{-Co(en)}_3][\ \Delta\text{-Co(en)(ox)}_2]I_2\cdot 3H_2O$ with hydrogen-bonding interactions shown as dotted lines. Iodide ions are shown as hatched circles.

ligand interacts through a terminal and a metal-bound oxygen with three protons on one of the C_3 faces of $[Co(en)_3]^{3+}$ (Figure 7a). The two sides of a single oxalate group are involved with different cations, and there is an additional interaction through both terminal oxygens along a C_2 axis of $[Co(en)_3]^{3+}$ with a Co–Co distance of 7.69 Å (Figure 7b). The second oxalate hydrogen bonds only through a terminal oxygen to a second

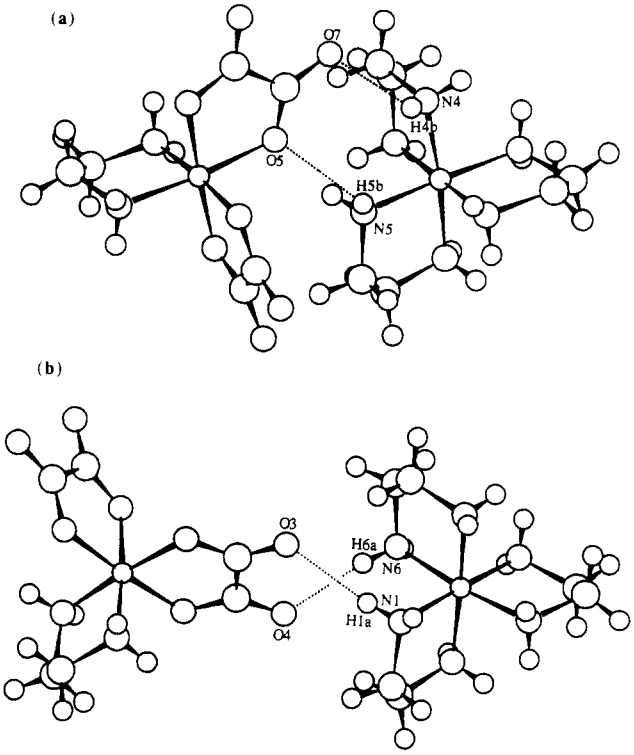

Figure 3. (a) Lateral hydrogen-bonding interaction for $[\Lambda\text{-Co(en)}_3][\Delta\text{-Co(en)(ox)}_2]I_2\cdot 3H_2O$, with a Co–Co distance of 6.13 Å. A similar interaction is found with a Co–Co distance of 6.15 Å. (b) Terminal hydrogen-bonding interaction for $[\Lambda\text{-Co(en)}_3][\Delta\text{-Co(en)(ox)}_2]I_2\cdot 3H_2O$, with a Co–Co distance of 7.55 Å. A similar interaction is found with a Co–Co distance of 7.53 Å.

Table V. Possible Hydrogen-Bonding Interactions in $[\Lambda\text{-}(+)_{589}\text{-Co(en)}_3][\Delta\text{-}(+)_{546}\text{-Co(en)(ox)}_2]I_2\cdot 3H_2O$

A···H–B	A–B, Å	A–H, (Å)	A–H–B, deg	Co–Co, Å
O7···H4b–N4	3.06	2.44	129.0	6.13
O5···H5b–N5	3.08	2.55	119.8	6.13
O3···H6b–N6	3.04	2.41	129.6	6.15
O1···H3b–N3	3.13	2.57	123.3	6.15
O7···H2a–N2	3.08	2.23	168.7	7.53
O8···H4a–N4	3.00	2.18	157.8	7.53
O3···H1a–N1	3.09	2.24	147.6	7.55
O4···H6a–N6	2.95	2.10	164.7	7.55
O3s···H7b–N7	2.90	2.13	146.2	
O2s···H7b–N7	3.06	2.32	143.3	
O6···H–O1s	2.91			
O8···H–O1s	3.06			
O8···H–O4s	3.11			

$[Co(gly)(ox)_2]^{2-}$ anion at Co-Co distances of 6.72 Å. These strong interactions involve double stacks of anions which are interwoven along the *b* axis of the crystal. The glycinate ligand of $[Co(gly)(ox)_2]^{2-}$ also forms hydrogen bonds along a C_2 axis of $[Co(en)_3]^{3+}$ with a Co–Co distance of 6.66 Å. A C_2 axis of $[Co(en)_3]^{3+}$ which is not involved in hydrogen bonding is blocked by the iodide ion. A list of possible hydrogen-bonding interactions in $[\Lambda\text{-Co(en)}_3][\Delta\text{-Co(gly)(ox)}_2]I\cdot H_2O$ is given in Table VII.

Discussion

While the individual component ions of the salts have normal bond lengths and angles, the interactions between these complex ions provide the primary focus of this paper. In all three structures, there is a complex pattern of hydrogen bonds between the ions and some common features are revealed. The anions $[Co(en)(ox)_2]^-$ and $[Co(gly)(ox)_2]^{2-}$ show two principal modes of hydrogen bonding interactions through oxalate to $[Co(en)_3]^{3+}$. At short Co–Co distances the interaction is through a terminal and a metal-bound oxygen, hereafter referred to as a "lateral" interaction, shown in Figures 3a, 5a, and 7a for the three salts. At longer

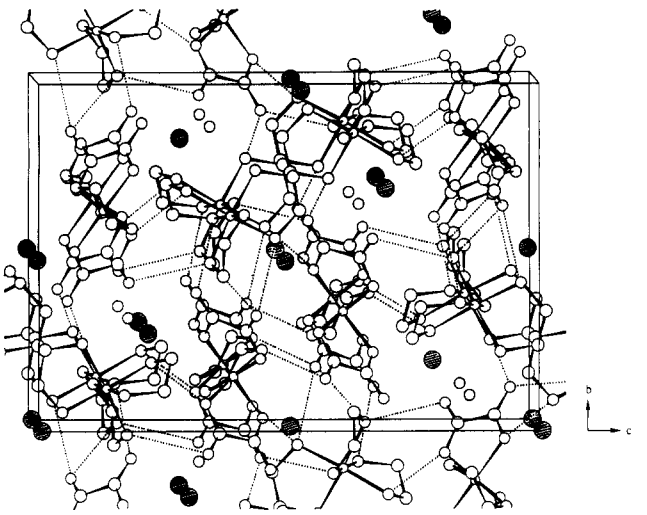

Figure 4. Packing diagram for $[\Delta\text{-Co(en)}_3][\Delta\text{-Co(en)(ox)}_2]I_2\cdot H_2O$ with hydrogen-bonding interactions shown as dotted lines. Iodide ions are shown as hatched circles.

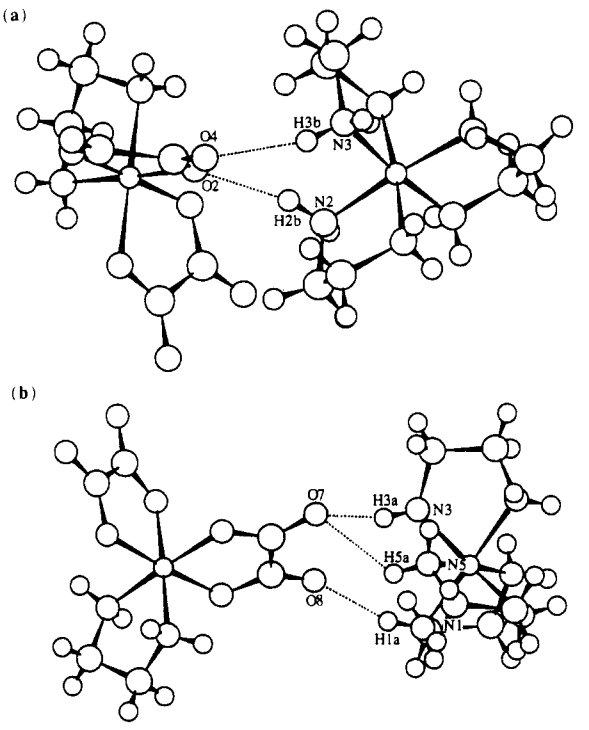

Figure 5. (a) Lateral hydrogen-bonding interaction for $[\Delta\text{-Co(en)}_3][\Delta\text{-Co(en)(ox)}_2]I_2\cdot H_2O$, with a Co–Co distance of 5.71 Å. A similar interaction is found with a Co–Co distance of 6.23 Å. (b) Terminal hydrogen-bonding interaction for $[\Delta\text{-Co(en)}_3][\Delta\text{-Co(en)(ox)}_2]I_2\cdot H_2O$, with a Co–Co distance of 7.23 Å.

Co-Co distances the interaction is through two terminal oxygen atoms as shown in Figures 3b, 5b and 7b, and hereafter referred to as a "terminal" interaction. Of the twelve amine protons of $[lel_3\text{-Co(en)}_3]^{3+}$ suitable for hydrogen bonding, six are directed along the C_3 axis of the complex with three on each face and the remaining six are distributed equally along the three C_2 axes. It is notable that, for the two $\Delta\Delta$ salts, the lateral interactions involve protons on the C_3 axis of $[Co(en)_3]^{3+}$ and the terminal interactions involve protons on a C_2 axis, while, for the $\Delta\Delta$ salt, the situation is reversed with lateral interactions involving the C_2 protons and terminal interactions involving the C_3 protons. This simple observation may well be germane to the mechanism of chiral discrimination in these systems. The helicity along the C_3 axis of $[\Delta\text{-Co(en)}_3]^{3+}$ is positive, $P(C_3)$, and along the C_2 axis is negative, $M(C_2)$.

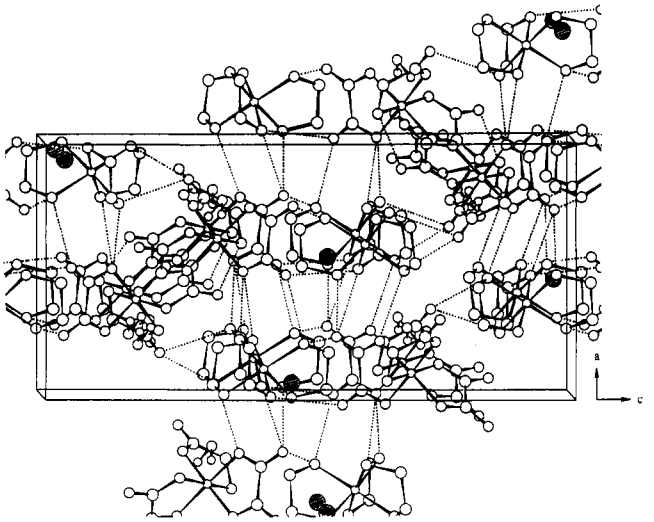

Figure 6. Packing diagram for $[\Lambda\text{-Co(en)}_3][\Delta\text{-Co(gly)(ox)}_2]I\cdot H_2O$ with hydrogen-bonding interactions shown as dotted lines. Iodide ions are shown as hatched circles.

Table VI. Possible Hydrogen-Bonding Interactions in $[\Delta\text{-}(-)_{589}\text{-Co(en)}_3][\Delta\text{-}(+)_{546}\text{-Co(en)(ox)}_2]I_2\cdot H_2O$

A···H–B	A–B, Å	A–H, Å	A–H–B, deg	Co–Co, Å
O4···H3b–N3	3.15	2.34	155.7	5.71
O2···H2b–N2	2.99	2.14	164.3	5.71
O3···H4b–N4	2.94	2.08	167.5	6.23
O1···H5b–N5	3.04	2.23	157.8	6.23
O8···H1a–N1	2.88	2.16	139.5	7.23
O7···H3a–N3	3.00	2.22	149.0	7.23
O7···H5a–N5	3.01	2.39	128.2	7.23
O3···H6b–N6	2.99	2.29	139.0	7.81
O7···H7a–N7	2.92	2.11	154.7	7.24
O1s···H2a–N2	3.01	2.23	150.1	
O1s···H4a–N4	3.02	2.19	159.0	
O1s···H6a–N6	3.17	2.37	153.9	
O8···H–O1s	3.08			

The manner in which chirality is communicated from one ion to another is most clearly demonstrated by the terminal interactions. For $\{[\Lambda\text{-Co(en)}_3]^{3+},[\Delta\text{-Co(en)(ox)}_2]^-\}$ and $\{[\Lambda\text{-Co(en)}_3]^{3+},[\Delta\text{-Co(gly)(ox)}_2]^{2-}\}$ the helical arrangement along the C_2 axis of the cation is propagated by two strong hydrogen bonds (Figures 3b and 7b), while for $\{[\Delta\text{-Co(en)}_3]^{3+},[\Delta\text{-Co(en)(ox)}_2]^-\}$ the hydrogen bonds are longer and the O–H–N angles are more acute (Figure 5b). A similar arrangement is noted in [*rac*-Co(en)$_3$](ox)I·1.5H$_2$O.[37]

As far as can be ascertained, there are no other examples of X-ray crystallographic studies of the mode of chiral discrimination between complex ions involving enantiomerically pure diastereomeric salts. Kuroda[14] has reported diastereomeric interactions involving $[\Lambda\text{-Co(en)}_3][\Delta\text{-Rh(ox)}_3]$ and $[\Delta\text{-Co(en)}_3][\Delta\text{-Rh(ox)}_3]$ in an optically impure crystal. In both cases, the ions interact along mutual C_3 axes with strong hydrogen bonding but the structure provides little evidence for the mechanism of discrimination (Figure 8). On the other hand, chiral discrimination in the interaction of the tartrate ion with $[Co(en)_3]^{3+}$ has been extensively investigated,[38,39] and this work has been extended to $[Co(sen)]^{3+}$ [40,41] and $[Co(chxn)_3]^{3+}$.[42-44] It has been suggested that the efficient chiral discrimination shown by the tartrate ion with these complexes is due to formation of a "local block" in

(40) Okazaki, H.; Sakaguchi, U.; Yoneda, H. *Inorg. Chem.* **1983**, *22*, 1539–1542.
(41) Bernal, I.; Korp, J. D.; Creaser, I. I. *Aust. J. Chem.* **1984**, *37*, 2365–2369.
(42) Mizuta, T.; Toshitani, K.; Miyoshi, K.; Yoneda, H. *Inorg. Chem.* **1990**, *29*, 3020–3026.
(43) Mizuta, T.; Toshitani, K.; Miyoshi, K. *Inorg. Chem.* **1991**, *30*, 572–574.
(44) Mizuta, T.; Toshitani, K.; Miyoshi, K. *Bull. Chem. Soc. Jpn.* **1991**, *64*, 1183–1191.

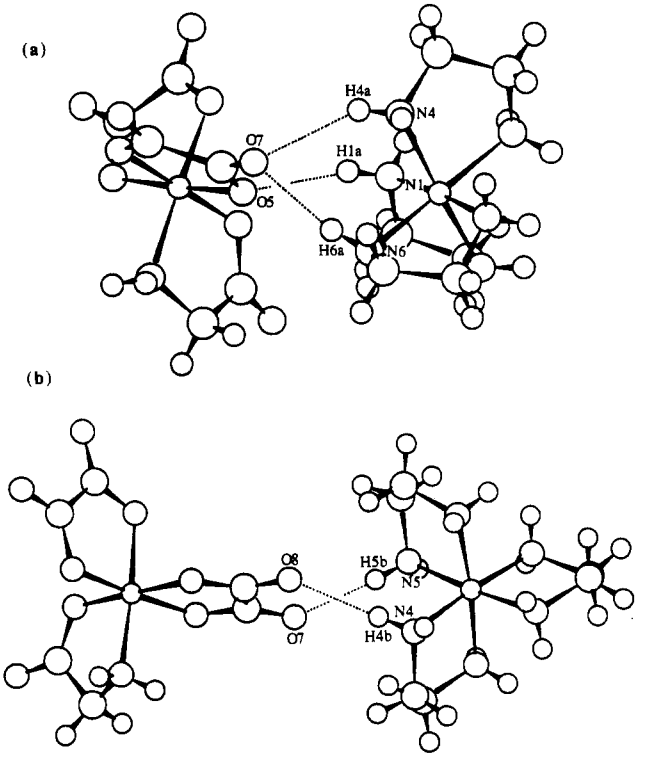

Figure 7. (a) Lateral hydrogen-bonding interaction for $[\Lambda\text{-Co(en)}_3][\Delta\text{-Co(gly)(ox)}_2]I\cdot H_2O$, with a Co–Co distance of 5.69 Å. A similar interaction is found with a Co–Co distance of 5.75 Å. (b) Terminal hydrogen-bonding interaction for $[\Lambda\text{-Co(en)}_3][\Delta\text{-Co(gly)(ox)}_2]I\cdot H_2O$, with a Co–Co distance of 7.69 Å.

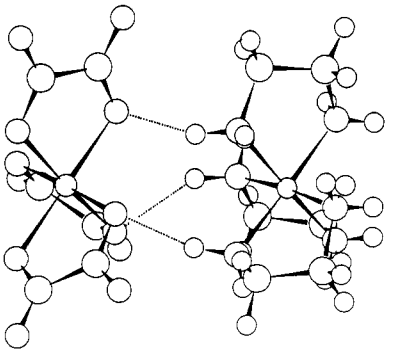

Figure 8. Hydrogen-bonding interactions in $[Rh(ox)_3][Co(en)_3]$, adapted from ref 14.

Table VII. Possible Hydrogen-Bonding Interactions in $[\Lambda\text{-}(+)_{589}\text{-Co(en)}_3][\Delta\text{-}(+)_{546}\text{-Co(gly)(ox)}_2]I\cdot H_2O$

A···H–B	A–B, Å	A–H, Å	A–H–B, deg	Co–Co, Å
O5···H1a–N1	3.03	2.19	161.8	5.69
O7···H4a–N4	3.08	2.40	134.3	5.69
O7···H6a–N6	2.95	2.13	157.5	5.69
O6···H2a–N2	3.04	2.21	160.4	5.75
O6···H3a–N3	3.22	2.44	149.7	5.75
O8···H5a–N5	2.94	2.12	158.1	5.75
O10···H1b–N1	2.92	2.12	154.8	6.66
O10···H3b–N3	3.01	2.17	165.4	6.66
O7···H5b–N5	2.90	2.09	153.1	7.69
O8···H4b–N4	3.06	2.19	168.5	7.69
O3···H7b–N7	2.86	2.00	169.8	6.72
O1s···H4a–N4	3.14	2.42	139.3	
O4···H1sa–O1s	2.86	1.97	157.1	
O1···H1sb–O1s	2.79	1.81	155.8	

which the tartrate ion directs its four almost coplanar oxygen atoms (two hydroxyl and two carboxylate) toward the three exposed amine groups on one of the C_3 faces of the cation. This hydrogen-bonding interaction is stronger for the less soluble diastereomers, $[\Lambda\text{-Co(en)}_3]^{3+}$, $[\Lambda\text{-Co(sen)}]^{3+}$, and [$\Lambda$-lel$_3$-Co-

$(S,S\text{-chxn})_3]^{3+}$ with *R,R*-tartrate. More effective discrimination is found with $[Co(chxn)_3]^{3+}$ and $[Co(pn)_3]^{3+}$ [45] and is ascribed to steric interference with the bulkier ligands, while the absence of any discrimination with $[Co(sep)]^{3+}$ is thought to be due to the absence of an available C_3 face.[45] Although this "local block" is clearly an essential feature of these crystals, it is by no means the only mode of hydrogen bonding.[46-49] In the present study, both C_3 and C_2 axes of $[Co(en)_3]^{3+}$ are heavily involved in hydrogen bonding interactions with the anions.

Chiral recognition in the interactions between $[Co(en)_3]^{3+}$ and $[Co(en)(ox)_2]^-$ has been examined in solution with use of chromatographic methods[9,10] which indicate that there is a modest preference for the ΔΔ diastereomeric pair. While it is unwise to emphasize comparisons of solution and crystallographic studies, it is noteworthy that the interactions at the closest Co–Co distance in the crystal structure, considered the most relevant to solution structure, involve stronger hydrogen bonds for the ΔΔ pair than for the ΔΛ pair. The ion $[Co(en)(ox)_2]^-$ belongs to the classification which has no C_3 carboxylate motif. The solution structure of the related ion pair $\{[Co(en)_3]^{3+}$, [*cis*-α-Co(edda)(ox)]$^-\}$ has been investigated by NMR and exhibits a weakly structured interaction which[7] is remarkably similar to the lateral interaction noted in the present work. The ion $[Co(gly)(ox)_2]^{2-}$ has the C_3 motif. Conductivity studies[18] of the ion pair with $[Co(en)_3]^{3+}$ in solution indicate a ΔΛ preference. The dominant solution structure for ion pairs containing the C_3 motif has also been examined by NMR methods to reveal a strong interaction with the pseudo-C_3 face of the anion, similar to the solid-state structure for $[Co(en)_3][Rh(ox)_3]$ evaluated by Kuroda. By way of contrast, the X-ray structure of [Λ-Co(en)$_3$][Δ-Co(gly)$(ox)_2]I\cdot H_2O$ shows no dominant interaction which can be ascribed to the pseudo-C_3 face of the anion. In fact, the interactions are of the lateral and terminal oxalate types found in the complexes of $[Co(en)(ox)_2]^-$. It would appear that, in this instance, the X-ray structure has less relevance to studies in solution although it must be recalled that the solution structure is an average of a dynamic assembly of microstructures.

It is of some interest to consider the relative importance of charge and hydrogen bonding in promoting interactions between the complex ions. Kuroda[14] has reported the structure of [Λ-Co(en)$_3$][Λ-Rh$(ox)_3$] and Butler and Snow[13] have reported the structure of [Δ-Co((−)-pn)$_3$][Λ-Cr$(mal)_3]\cdot 3H_2O$, two complexes in which both cation and anion are triply charged. The shortest Co–Rh distance reported in the former case is 4.91 Å, and the shortest Co–Cr distance in the latter case is 5.03 Å. In both instances, the cation and anion are strongly hydrogen bonded to each other through their respective C_3 faces. Lethbridge and co-workers[15] have reported the structure of $[Cr(en)_2(ox)][Cr(en)(ox)_2]\cdot 2H_2O$, which has a minimum Cr–Cr distance of 5.45 Å. The longer minimum metal–metal distance is to be expected from the lower charge product; however the cation and anion remain strongly hydrogen-bonded to each other along their respective pseudo-C_3 axes. Similar effects would be expected for [Λ-Co(en)$_3$][Δ-Co(gly)$(ox)_2]I\cdot H_2O$, where the charge product is high, and the potential for C_3–C_3 hydrogen-bonding interactions has been shown by NMR.[7] However such an interaction is absent, and the shortest Co–Co distance is 5.69 Å. The most likely explanation of this is the presence of the iodide anions, necessary for charge balance but apparantly disruptive to optimal hydrogen-bonding interactions.

Acknowledgment. The support of the National Science Foundation (Grant No. CHE 90–16682) is gratefully acknowledged.

Supplementary Material Available: Lists of fractional coordinates and isotropic displacement parameters for the hydrogen atoms, selected interatomic distances, selected interatomic angles, and general atomic displacement parameters and ORTEP drawings of the complex ions showing the atom-numbering schemes (Figures SI–SVI) (22 pages). Ordering information is given on any current masthead page.

(45) Sakaguchi, U.; Tsuge, A.; Yoneda, H. *Inorg. Chem.* **1983**, *22*, 1630–1634.
(46) Kuramoto, M.; Kushi, Y.; Yoneda, H. *Bull. Chem. Soc. Jpn.* **1978**, *51*, 3251–3256.
(47) Kuramoto, M.; Kushi, Y.; Yoneda, H. *Bull. Chem. Soc. Jpn.* **1980**, *53*, 125–132.
(48) Kuramoto, M. *Bull. Chem. Soc. Jpn.* **1979**, *52*, 3702–3712.
(49) Geue, R. J.; Snow, M. R. *Inorg. Chem.* **1977**, *16*, 231–241.